Harmonic Total Concurrence: A Bottleneck-Sensitive Genuine Multipartite Entanglement Measure

Qi Han(韩琦)[a,b,*], Xuexin Huang(黄学鑫)[a,§], Junlin Li(李君临)[a,†], and Xiao Wu(吴晓)[a,‡]

[a] *College of Mathematics and Statistics, Northwest Normal University*

[b] *Gansu Provincial Research Center for Basic Disciplines of Mathematics and Statistics, Lanzhou, 730070, China*

[a,b,*] *hanqi1978@nwnu.edu.cn,* [a,§] *2066725368@qq.com,* [a,†] *2486058248@qq.com,*

[a,‡] *2728353765@qq.com*

Received Day Month Year
Revised Day Month Year

Quantum entanglement is a core resource for quantum communication and computation. Genuine multipartite entanglement (GME), as a critical quantum correlation, underpins measurement-based quantum computation and multipartite quantum simulation, but existing GME measures cannot well characterize uneven entanglement distributions and are insensitive to single-partition entanglement failure in practical bottleneck scenarios. To address this problem, we propose a novel GME measure termed harmonic total concurrence (HTC), defined as the harmonic mean of total concurrence over all nontrivial bipartitions, and place it within a one-parameter power-mean family of total concurrence measures. HTC satisfies the standard entanglement hierarchy and effectively distinguishes GHZ and W states. Its computable lower bounds for mixed states outperform geometric total concurrence in entanglement detection under typical noise, and it extends the effective time window for entanglement certification while enabling early warning of asymmetric entanglement decay. We further define an entanglement non-uniformity parameter and prove HTC induces a state ordering distinct from existing measures. This work provides a new theoretical tool for multipartite entanglement characterization, with good experimental accessibility on photonic, atomic and optomechanical platforms.

Keywords: harmonic total concurrence; genuine multipartite entanglement measure; bottleneck sensitivity; entanglement distribution

PACS: 03.67.Mn, 03.65.Ud, 03.67.-a

1. Introduction

Quantum entanglement is a cornerstone of quantum information science and the core resource for quantum communication and quantum computation protocols. It finds wide applications in quantum key distribution [1,2], dense coding [2], quantum teleportation [3] and quantum secret sharing [4]. In multipartite systems, genuine multipartite entanglement (GME) refers to entanglement that cannot be expressed as a convex mixture of states that are separable with respect to any bipartition. It serves as an essential resource for measurement-based quantum computation [5,6], offers advantages in quantum error correction, and plays a key role in simulating

strongly correlated multipartite systems [7]. Consequently, the quantification of GME has become an important research objective [8, 9].

For bipartite systems, researchers have proposed various entanglement measures. These include the concurrence and entanglement of formation for two-qubit entanglement [10, 11], as well as the negativity [12]. High-dimensional generalizations of these quantities have also been constructed [13]. Further studies have proposed parameterized generalizations including the q-concurrence [14] with $q \geq 2$ and the α-concurrence [15] with $0 \leq \alpha \leq 1/2$. Such quantities allow a more flexible description of different properties of bipartite quantum correlations and lay the foundation for the study of multipartite entanglement.

However, characterizing GME in multipartite systems is more complex. The generalized geometric measure [16, 17] is defined as the geometric distance from a given state to the set of biseparable states, whereas the GME-concurrence (GMC) [18] is given by the minimum bipartite concurrence over all bipartitions. Related geometric constructions include the geometric mean of bipartite concurrences [19], its q-concurrence generalization [20], the concurrence fill for tripartite systems [21], and the informationally complete entanglement measure [22]. Further parameterized measures have been proposed, such as the q-k-ME concurrence and α-k-ME concurrences [23], together with the geometric mean of α-concurrence [24]. Recently, Xuan *et al.* [25] defined the total concurrence for bipartite systems, and Liang *et al.* [26] constructed the geometric total concurrence (GTC) by evaluating the geometric mean of total concurrences over all bipartitions.

Despite these advances, many existing entanglement measures rely on either the minimum or the geometric mean of bipartite entanglements, both of which have obvious limitations. The GMC only considers the weakest bipartition and ignores other partitions; the GTC adopts the geometric mean, which allows strongly entangled bipartitions to offset weakly entangled ones and conceal unbalanced entanglement distributions. Such quantification measures fail in bottleneck scenarios, where the overall performance is limited by the weakest entanglement. For instance, the end-to-end fidelity of quantum repeater chains is bounded by the weakest link [27], while the logical error rate of measurement-based quantum computation is determined by the most noisy entangled resource [5, 6]. A measure that penalizes heterogeneous entanglement distributions and vanishes whenever a single partition fails to be entangled is therefore desirable.

In this paper, we construct a GME measure, the harmonic total concurrence (HTC), by taking the harmonic mean of the total concurrence over all nontrivial bipartitions, and place it within a one-parameter power-mean family of total concurrences. The HTC respects the hierarchy that assigns a higher value to the GHZ state than to the W state. For mixed states, we derive computable lower bounds for the mixed-state HTC, which deliver better GME detection than GTC bounds under typical noise scenarios. Then we examine entanglement evolution in three representative dynamical processes, demonstrating that the HTC-based witness prolongs

the effective time interval for entanglement certification and delivers early warning of entanglement decay under asymmetric dissipation. To characterize the distributional heterogeneity of entanglement across cuts, we define the entanglement non-uniformity parameter η_q. Through comparative case investigations, we demonstrate that the HTC induces an ordering of entangled states that is inequivalent to those induced by the GMC and the GTC.

The paper is organized as follows. Section 2 reviews the total concurrence and the power-mean formalism. Section 3 presents the definition of the HTC, proves its validity as a GME measure, and discusses its position within the power-mean family of total concurrences. Section 4 constructs SDP-based lower bounds for mixed states and compares their detection performance. Section 5 analyzes entanglement evolution in three representative dynamical processes. Section 6 discusses the entanglement ordering properties induced by this measure and introduces an entanglement nonuniformity parameter. Section 7 concludes the paper.

2. Preliminaries

We consider an n-partite quantum system with constituents $A_1, \ldots, A_n$ and total Hilbert space $\mathcal{H} = \bigotimes_{i=1}^{n} \mathcal{H}_{A_i}$, where $\dim \mathcal{H}_{A_i} = d_i$. A nontrivial bipartition (or cut) γ is an unordered decomposition of the index set $\{1, \ldots, n\}$ into two nonempty disjoint subsets S_γ and $\bar{S}_\gamma$. The collection of all such cuts is denoted by Γ_n; its cardinality is

$$|\Gamma_n| = \mathfrak{N}_n = \begin{cases} \displaystyle\sum_{m=1}^{(n-1)/2} \binom{n}{m}, & \text{if } n \text{ is odd}, \\ \displaystyle\sum_{m=1}^{(n-2)/2} \binom{n}{m} + \frac{1}{2}\binom{n}{n/2}, & \text{if } n \text{ is even}. \end{cases} \tag{1}$$

For each $\gamma \in \Gamma_n$, the Hilbert space factorizes as $\mathcal{H} = \mathcal{H}_{S_\gamma} \otimes \mathcal{H}_{\bar{S}_\gamma}$, and we define the local dimension $\delta_\gamma = \min\{\dim \mathcal{H}_{S_\gamma}, \dim \mathcal{H}_{\bar{S}_\gamma}\}$. For a pure state $|\psi\rangle \in \mathcal{H}$, the reduced state of S_γ is $\rho_{S_\gamma} = \mathrm{Tr}_{\bar{S}_\gamma}(|\psi\rangle\langle\psi|)$.

A legitimate measure of GME is a functional $\mathcal{E}$ on quantum states satisfying four fundamental criteria [21,28]: (A1) $\mathcal{E}$ vanishes on all biseparable and fully separable states; (A2) $\mathcal{E}$ is strictly positive on all non-biseparable states; (A3) $\mathcal{E}$ is non-increasing under local operations and classical communication (LOCC); and (A4) $\mathcal{E}(|\mathrm{GHZ}_n\rangle) > \mathcal{E}(|\mathrm{W}_n\rangle)$ for all $n \geq 3$, reflecting the operational distinction between these paradigmatic states. While (A1)-(A3) ensure that $\mathcal{E}$ detects and quantifies GME, criterion (A4) demands that the measure discriminates between qualitatively different entanglement structures.

To construct such a measure, we require a bipartite entanglement monotone that can be evaluated across every cut. The total concurrence of order $q \geq 2$ serves this purpose [25]. For a bipartite pure state $|\phi\rangle \in \mathcal{H}_A \otimes \mathcal{H}_B$, let $d = \min\{\dim \mathcal{H}_A, \dim \mathcal{H}_B\}$. Without loss of generality, assume $\dim \mathcal{H}_A = d$ and define

$\rho_A = \mathrm{Tr}_B\,|\phi\rangle\langle\phi|$. The total concurrence is then defined as

$$\mathfrak{T}_q(|\phi\rangle) = \frac{d - \mathrm{Tr}(\rho_A^q) - \mathrm{Tr}(\mathbb{I}_d - \rho_A)^q}{\Lambda_q(d)}, \tag{2}$$

where the normalization $\Lambda_q(d) = d - d^{1-q}[1 + (d-1)^q]$ ensures $\mathfrak{T}_q \in [0,1]$. This symmetry between ρ_A and $\mathbb{I}_d - \rho_A$ makes the measure cut-invariant. For mixed states, $\mathfrak{T}_q$ is extended via the convex roof. We know that $\mathfrak{T}_q$ vanishes for separable states, takes strictly positive values for entangled pure states, and is monotonic under LOCC. In the multipartite setting, for a pure state $|\psi\rangle$ and a cut $\gamma \in \Gamma_n$, we write $\mathfrak{T}_q^{(\gamma)}(|\psi\rangle) \equiv \mathfrak{T}_q(|\psi\rangle_{S_\gamma|\bar{S}_\gamma})$ with local dimension δ_γ. We refer to the collection $\{\mathfrak{T}_q^{(\gamma)}(|\psi\rangle)\}_{\gamma\in\Gamma_n}$ as the entanglement distribution across all nontrivial bipartitions of $|\psi\rangle$.

Our aim is to combine this distribution into a single scalar that respects the GME axioms. Existing approaches rely on the minimum or the geometric mean across cuts. To transcend these extremes, we invoke the power means (Hölder means). For a vector $\mathbf{x} \in \mathbb{R}_{>0}^N$, where $\mathbb{R}_{>0}^N$ denotes the set of N-dimensional vectors with strictly positive real entries, and $p \in \mathbb{R} \setminus \{0\}$,

$$\mathcal{M}_p(\mathbf{x}) = \left(\frac{1}{N}\sum_{i=1}^{N} x_i^p\right)^{1/p}, \tag{3}$$

with continuous extensions $\mathcal{M}_0(\mathbf{x}) = (\prod_i x_i)^{1/N}$ and $\mathcal{M}_{-\infty}(\mathbf{x}) = \min_i x_i$. The power-mean inequality states that for $p < r$,

$$\mathcal{M}_p(\mathbf{x}) \le \mathcal{M}_r(\mathbf{x}), \tag{4}$$

with equality if and only if all components are identical. The harmonic mean $\mathcal{H}(\mathbf{x}) \equiv \mathcal{M}_{-1}(\mathbf{x}) = \left[\frac{1}{N}\sum_i x_i^{-1}\right]^{-1}$ has two properties essential for entanglement theory. First, it is strictly Schur-concave: for fixed arithmetic mean, $\mathcal{H}(\mathbf{x})$ is minimized when the distribution is maximally heterogeneous. Consequently, it penalizes states in which entanglement is concentrated on a few cuts while others are weakly entangled. Second, $\mathcal{H}(\mathbf{x}) \to 0$ whenever any component $x_j \to 0^+$, regardless of the remaining components. This mirrors the physical bottleneck principle that a quantum network is only as robust as its weakest entanglement link. These mathematical features motivate the construction of a GME measure based on the harmonic mean of the entanglement distribution, which we will introduce in the following section.

3. Harmonic total concurrence

In a protocol that needs entanglement across every bipartition, one separable cut already removes GME from the global state, so a measure must be sensitive to the weakest cut while still using the information carried by the others. The power-mean formalism of Sec. 2 demonstrates that the harmonic mean is the suitable average for entanglement distributions subject to this bottleneck effect. We now elaborate this construction and prove that it is a legitimate GME measure. In addition, we

incorporate the HTC into the power-mean family of total concurrence and clarify its special nature.

3.1. *Definition and axiomatic properties*

For an n-partite pure state $|\psi\rangle \in \mathcal{H}$ with entanglement distribution $\{\mathfrak{T}_q^{(\gamma)}(|\psi\rangle)\}_{\gamma\in\Gamma_n}$, the harmonic total concurrence (HTC) of $q \geq 2$ is defined as

$$\mathcal{H}_q(|\psi\rangle) = \begin{cases} \left[\dfrac{1}{\mathfrak{N}_n}\displaystyle\sum_{\gamma\in\Gamma_n}\dfrac{1}{\mathfrak{T}_q^{(\gamma)}(|\psi\rangle)}\right]^{-1}, & \mathfrak{T}_q^{(\gamma)}(|\psi\rangle) > 0 \text{ for all } \gamma \in \Gamma_n, \\ 0, & \text{otherwise.} \end{cases} \tag{5}$$

The condition $\mathfrak{T}_q^{(\gamma)} > 0$ for all γ is equivalent to GME, since the vanishing of any single bipartite total concurrence signals biseparability across that cut.

In structured systems such as quantum networks, not all bipartitions carry equal operational weight. Let $\{w_\gamma\}_{\gamma\in\Gamma_n}$ be a probability distribution over cuts. The weighted harmonic total concurrence (WHTC) is

$$\mathcal{H}_q^{(w)}(|\psi\rangle) = \begin{cases} \left[\displaystyle\sum_{\gamma\in\Gamma_n}\dfrac{w_\gamma}{\mathfrak{T}_q^{(\gamma)}(|\psi\rangle)}\right]^{-1}, & \mathfrak{T}_q^{(\gamma)}(|\psi\rangle) > 0 \text{ for all } \gamma, \\ 0, & \text{otherwise.} \end{cases} \tag{6}$$

The weights may encode spatial separation, communication cost, or topological centrality of subsystems. Setting $w_\gamma = 1/\mathfrak{N}_n$ recovers the uniform HTC.

For mixed states ρ, we extend $\mathcal{H}_q$ via the convex-roof construction,

$$\mathcal{H}_q(\rho) = \inf_{\{p_i,|\psi_i\rangle\}} \sum_i p_i\, \mathcal{H}_q(|\psi_i\rangle), \tag{7}$$

where the infimum runs over all pure-state ensembles $\rho = \sum_i p_i|\psi_i\rangle\langle\psi_i|$.

We now verify that $\mathcal{H}_q$ satisfies the four axiomatic requirements (A1)-(A4) for a GME measure.

Theorem 1. *The harmonic total concurrence $\mathcal{H}_q$ defined in Eqs.* (5)-(7) *is a valid measure of genuine multipartite entanglement for any n-partite quantum system.*

Proof. We examine each criterion in turn.

(A1)-(A2). Eq. (5) yields $\mathcal{H}_q = 0$ exclusively on biseparable pure states. Via the convex-roof extension (7), every biseparable mixed state attains zero, while genuine multipartite entangled states acquire strictly positive values because $\mathcal{H}_q$ is continuous on pure states and the set of biseparable pure states is closed.

(A3). For any fixed cut γ, the bipartite total concurrence $\mathfrak{T}_q^{(\gamma)}$ is an entanglement monotone: it does not increase under LOCC acting on the subsystems of the cut. The function $f : \mathbb{R}_{>0}^{\mathfrak{N}_n} \to \mathbb{R}_{>0}$, where $\mathbb{R}_{>0}^{\mathfrak{N}_n}$ denotes the set of $\mathfrak{N}_n$-dimensional vectors

with strictly positive real entries, is defined by $f(\mathbf{x}) = \left[\frac{1}{\mathfrak{N}_n}\sum_i x_i^{-1}\right]^{-1}$. This function is strictly increasing in each argument, since $\partial f/\partial x_j = f(\mathbf{x})^2/(\mathfrak{N}_n x_j^2) > 0$. Therefore, if an LOCC operation Λ yields $\mathfrak{T}_q^{(\gamma)}(\Lambda(\rho)) \leq \mathfrak{T}_q^{(\gamma)}(\rho)$ for all γ, then $\mathcal{H}_q(\Lambda(\rho)) \leq \mathcal{H}_q(\rho)$. The convex-roof extension preserves this monotonicity, establishing (A3).

(A4). Consider the n-qubit GHZ state $|\mathrm{GHZ}_n\rangle = \frac{1}{\sqrt{2}}(|0\rangle^{\otimes n} + |1\rangle^{\otimes n})$ and the W state $|\mathrm{W}_n\rangle = \frac{1}{\sqrt{n}}\sum_{j=1}^{n}|0\rangle^{\otimes(j-1)} \otimes |1\rangle \otimes |0\rangle^{\otimes(n-j)}$. For $|\mathrm{GHZ}_n\rangle$, every bipartition yields the same reduced density matrix $\rho_{S_\gamma} = \frac{1}{2}(|0\rangle\langle 0| + |1\rangle\langle 1|)$, so the entanglement spectrum is constant: $\mathfrak{T}_q^{(\gamma)}(|\mathrm{GHZ}_n\rangle) = \mathfrak{t}_{\mathrm{GHZ}}$ for all γ. Consequently,

$$\mathcal{H}_q(|\mathrm{GHZ}_n\rangle) = \mathcal{T}_q(|\mathrm{GHZ}_n\rangle) = \mathfrak{t}_{\mathrm{GHZ}}, \tag{8}$$

where $\mathcal{T}_q$ denotes the GTC. For $|\mathrm{W}_n\rangle$, the reduced states depend on the size of S_γ, producing a non-constant entanglement distribution. By the strict power-mean inequality $\mathcal{M}_{-1} < \mathcal{M}_0$ for non-uniform vectors,

$$\mathcal{H}_q(|\mathrm{W}_n\rangle) < \mathcal{T}_q(|\mathrm{W}_n\rangle). \tag{9}$$

Reference [26] has shown that $\mathcal{T}_q(|\mathrm{W}_n\rangle) < \mathcal{T}_q(|\mathrm{GHZ}_n\rangle)$ for all $n \geq 3$ and $q \geq 2$. Chaining these inequalities yields

$$\mathcal{H}_q(|\mathrm{W}_n\rangle) < \mathcal{T}_q(|\mathrm{W}_n\rangle) < \mathcal{T}_q(|\mathrm{GHZ}_n\rangle) = \mathcal{H}_q(|\mathrm{GHZ}_n\rangle), \tag{10}$$

which confirms (A4). □

The proof of (A4) reveals a key feature of the harmonic mean: it is more sensitive to uneven entanglement distributions. The W state has a nonuniform distribution, which reduces its HTC below its GTC. The GHZ state has a uniform distribution, so its HTC equals its GTC. This creates a strict hierarchy among power averages. We define the arithmetic total concurrence (ATC) as $\mathcal{A}_q(|\psi\rangle) = \frac{1}{\mathfrak{N}_n}\sum_\gamma \mathfrak{T}_q^{(\gamma)}(|\psi\rangle)$. Then we have the following ordering.

Proposition 1 (HM–GM–AM entanglement inequality). *For any genuinely multipartite entangled pure state* $|\psi\rangle$*,*

$$\mathcal{H}_q(|\psi\rangle) \leq \mathcal{T}_q(|\psi\rangle) \leq \mathcal{A}_q(|\psi\rangle), \tag{11}$$

with equality if and only if the entanglement distribution is constant over all $\gamma \in \Gamma_n$*.*

Proof. This follows immediately from the power-mean inequality $\mathcal{M}_{-1} \leq \mathcal{M}_0 \leq \mathcal{M}_1$ applied to the positive vector $(\mathfrak{T}_q^{(\gamma)})_{\gamma\in\Gamma_n}$, with equality only when all components are identical. □

Proposition 1 gives a three-tiered characterization of entanglement: $\mathcal{H}_q$ measures the bottleneck entanglement (the weakest link), $\mathcal{T}_q$ measures the typical entanglement (geometrically averaged performance), and $\mathcal{A}_q$ measures the aggregate entanglement (total resource pooled across cuts).

From a physical standpoint, the harmonic mean is the appropriate average when the performance of a composite system is limited by its weakest component. In quantum communication networks, the end-to-end fidelity across a repeater chain is bounded above by the fidelity of the least reliable link; similarly, in measurement-based quantum computation, the logical error rate is dominated by the noisiest entangled resource, not by the average noise level. Such noisy multipartite entangled resources have been experimentally realized on a growing range of platforms, including steady-state optical-mode entanglement in imperfect optomechanical nanobeams and Gaussian entanglement in coupled optomechanical resonators via photon hopping [29,30]. Certifying these resources for network or computation tasks therefore requires precisely the weakest-cut sensitivity that the HTC provides. The HTC incorporates this bottleneck principle: if a single bipartition becomes nearly separable, the harmonic mean becomes very small, signaling that the state's multipartite utility is compromised by one fragile cut. By contrast, the geometric mean weights every bipartition multiplicatively and may remain non-negligible for states that combine several highly entangled cuts with one weakly entangled cut—a structural weakness that the HTC correctly penalizes as insufficient for robust genuine multipartite entanglement.

3.2. *Power-mean family and the distinguished HTC*

The HTC is the $p = -1$ member of a continuous family of power-mean total concurrences. This family unifies the existing aggregations and clarifies the distinguished role of the HTC among them.

For $p \in \mathbb{R} \cup \{-\infty\}$, define the power-mean total concurrence of order q as

$$\mathcal{E}_{p,q}(|\psi\rangle) = \mathcal{M}_p\Big(\big(\mathfrak{T}_q^{(\gamma)}(|\psi\rangle)\big)_{\gamma\in\Gamma_n}\Big), \tag{12}$$

where $\mathcal{M}_p$ denotes the power mean of Eq. (3), and we set $\mathcal{E}_{p,q} = 0$ whenever any per-cut total concurrence vanishes. This family recovers the four most widely used GME measures as special cases:

$$\mathcal{E}_{-\infty,q} = C_{\mathrm{GME}}, \qquad \mathcal{E}_{-1,q} = \mathcal{H}_q \,(\mathrm{HTC}), \qquad \mathcal{E}_{0,q} = \mathcal{T}_q \,(\mathrm{GTC}), \qquad \mathcal{E}_{1,q} = \mathcal{A}_q \,(\mathrm{ATC}). \tag{13}$$

Theorem 2. *For every $p \in [-\infty, 0]$ and $q \geq 2$, $\mathcal{E}_{p,q}$ extended by the convex roof is a GME measure satisfying (A1)–(A4). For $p > 0$ it violates (A1).*

Proof. (A1)–(A2). For $p < 0$, if $\mathfrak{T}_q^{(\gamma_0)} = 0$ for some cut γ_0, the definition sets $\mathcal{E}_{p,q} = 0$. For $p = 0$ the product vanishes, and for $p = -\infty$ the minimum vanishes. On a genuinely multipartite entangled state every component is positive, all power means are positive, and continuity together with the closedness of the biseparable set carries this through the convex roof, as in Theorem 1.

(A3). Every power mean with $p \leq 1$ is symmetric, concave, and non-decreasing in each argument (monotone at $p = -\infty$). Componentwise LOCC monotonicity of the bipartite total concurrences and the convex roof give the result.

(A4). We compare the two states cut by cut. On a $k|n-k$ bipartition the GHZ reduction has spectrum $\{1/2, 1/2, 0, \ldots\}$ while the W reduction has spectrum $\{k/n, (n-k)/n, 0, \ldots\}$. For a rank-two reduced spectrum $\{\lambda, 1-\lambda, 0, \ldots\}$, the sum $\lambda^q + (1-\lambda)^q$ is minimized at $\lambda = 1/2$; the total concurrence $\mathfrak{T}_q$ of a rank-two state is correspondingly maximized at $\lambda = 1/2$. Hence

$$\mathfrak{T}_q^{(\gamma)}(|\mathrm{GHZ}_n\rangle) \geq \mathfrak{T}_q^{(\gamma)}(|\mathrm{W}_n\rangle)$$

on every cut, with strict inequality on the $1|n-1$ cuts for $n \geq 3$. Every symmetric aggregation that is non-decreasing in each argument—including the harmonic mean, the geometric mean, and every power mean with $p \leq 0$—therefore satisfies

$$\mathcal{E}_{p,q}(|\mathrm{GHZ}_n\rangle) > \mathcal{E}_{p,q}(|\mathrm{W}_n\rangle), \tag{14}$$

where the strict inequality follows from the strict increase on at least one cut. The endpoint $p = -\infty$ follows by continuity of the power mean,

$$\lim_{p\to-\infty} \left(\frac{1}{N} \sum_{i=1}^{N} x_i^p \right)^{1/p} = \min_i x_i, \tag{15}$$

under which the weakest component dominates the reciprocal-power sum.

Failure for $p > 0$. Consider the three-qubit biseparable state

$$|\chi\rangle = |\Phi^+\rangle_{12} \otimes |0\rangle_3 = \frac{1}{\sqrt{2}}(|000\rangle + |110\rangle), \tag{16}$$

separable across $12|3$ but entangled across $1|23$ and $2|13$. Tracing out qubit 3 leaves $|\Phi^+\rangle\langle\Phi^+|$ on qubits 1 and 2, so the one-qubit reductions of qubits 1 and 2 are each $\mathbb{I}_2/2$ and the concurrence is 1 on both cuts $1|23$ and $2|13$; across $12|3$ the reduction is $|0\rangle\langle 0|$ with concurrence 0. For $q = 2$ the total concurrences are $(1, 1, 0)$, so

$$\mathcal{E}_{p,2}(|\chi\rangle) = \left[\frac{1}{3}(1^p + 1^p + 0^p) \right]^{1/p} = \left(\frac{2}{3} \right)^{1/p} > 0 \quad (p > 0), \tag{17}$$

although $|\chi\rangle$ is biseparable. Every member with $p > 0$, including the ATC, therefore assigns a positive value to a biseparable state and violates (A1); such functionals quantify average rather than genuine multipartite entanglement.

The limit $\lim_{p\to 0^+} \mathcal{E}_{p,2}(|\chi\rangle) = \lim_{p\to 0^+} (2/3)^{1/p} = 0$ equals $\mathcal{E}_{0,2}(|\chi\rangle) = 0$, so the family is continuous in value at $p = 0$. Nevertheless the boundary member $p = 0$ vanishes on biseparable states, whereas every member with $p > 0$, however small, assigns $|\chi\rangle$ a strictly positive value; the validity interval therefore ends at, and includes, $p = 0$. □

Not every member of this family qualifies as a GME measure. Theorem 2 delineates the exact validity interval: every member with $p \in [-\infty, 0]$ satisfies all four GME axioms (A1)–(A4), whereas every member with $p > 0$ violates axiom (A1) by assigning strictly positive values to biseparable states. The harmonic mean $p = -1$ therefore lies strictly inside the valid regime, together with the geometric mean and the minimum-based measure.

The distinction between the valid members is qualitative, not merely quantitative. As the exponent p decreases from 0 to $-\infty$, the aggregation continuously shifts its weight from the collective average of all cuts to the single weakest cut. At $p = 0$ (the GTC), the geometric mean combines the per-cut values multiplicatively. A strongly entangled cut can thus compensate a nearly separable one, and the measure remains largely insensitive to how unevenly entanglement is distributed across bipartitions. At the opposite extreme, $p = -\infty$ (the GMC) retains only the minimum concurrence across all cuts and discards all information about the remaining ones; it cannot distinguish a state with one vanishing cut from a state where all cuts are equally weak.

The HTC at $p = -1$ occupies a unique intermediate position that neither endpoint achieves. Its reciprocal-sum form retains every cut in the aggregation, so that the overall value reflects the full distribution of entanglement across bipartitions. At the same time, any single cut approaching zero drives the whole mean to zero, ensuring that the measure vanishes exactly on biseparable states. More precisely, among all valid power means, the HTC is the most strictly Schur-concave one that still draws on every bipartition. It responds most strongly to a nearly separable cut—the bottleneck of the system—while preserving the contributions of all other cuts. This bottleneck sensitivity is precisely the property required by any protocol that demands entanglement across every bipartition, and it is what allows the HTC to order states that the GTC and GMC cannot distinguish (Sec. 5).

4. Lower bounds for the HTC on mixed states

The convex-roof definition of HTC requires optimization over all pure-state decompositions, which is computationally intractable for generic mixed states. To address this challenge, we construct computable lower bounds for the HTC using semidefinite programming (SDP)-based entanglement witnesses [31, 32], and evaluate their performance across paradigmatic noisy states, under local noise channels, and in realistic dynamical scenarios.

For a fixed bipartition $\gamma \in \Gamma_n$, let $\mathcal{W}_\gamma$ denote the set of normalized entanglement witnesses for the cut $S_\gamma|\bar{S}_\gamma$:

$$\mathcal{W}_\gamma = \big\{W_\gamma = W_\gamma^\dagger \,\big|\, \mathrm{Tr}(W_\gamma\sigma) \geq 0 \text{ for all separable } \sigma,\ \|W_\gamma\|_\infty \leq 1\big\}.$$

The boundedness condition ensures that the optimal violation

$$\epsilon_\gamma(\rho) = \max\Big\{0,\ -\min_{W_\gamma \in \mathcal{W}_\gamma} \mathrm{Tr}(W_\gamma\rho)\Big\} \tag{18}$$

is well defined and computable via standard SDP hierarchies. Since $\mathfrak{T}_q^{(\gamma)}$ is convex and vanishes exactly on the set of separable states, there exists a monotonically increasing function $f_{\gamma,q} : \mathbb{R}_{\geq 0} \to \mathbb{R}_{\geq 0}$, depending on the local dimension δ_γ and the order q, such that

$$\mathfrak{T}_q^{(\gamma)}(\rho) \geq f_{\gamma,q}\big(\epsilon_\gamma(\rho)\big). \tag{19}$$

For $q = 2$ the explicit form is $f_{\gamma,2}(\epsilon) = \delta_\gamma \epsilon^2 / \big[(\delta_\gamma - 1)(1+\epsilon)\big]$ [33]. For general q, $f_{\gamma,q}$ is obtained by inverting the Legendre-Fenchel transform of $\mathfrak{T}_q^{(\gamma)}$ restricted to the witness hyperplane [34, 35].

The harmonic mean is strictly increasing in each argument. Combining this monotonicity with (19) yields the following lower bound.

Theorem 3 (HTC lower bound via SDP witnesses). *Let ρ be an n-partite mixed state. For each $\gamma \in \Gamma_n$, let $\epsilon_\gamma(\rho)$ be given by* (18)*. Then*

$$\mathcal{H}_q(\rho) \geq \left[\frac{1}{\mathfrak{N}_n} \sum_{\gamma \in \Gamma_n} \frac{1}{f_{\gamma,q}\big(\epsilon_\gamma(\rho)\big)} \right]^{-1}. \tag{20}$$

If $\epsilon_\gamma(\rho) = 0$ for any γ, the right-hand side vanishes, consistent with $\mathcal{H}_q(\rho) = 0$.

Proof. From inequality (19), we obtain $\mathfrak{T}_q^{(\gamma)}(\rho) \geq y_\gamma \equiv f_{\gamma,q}(\epsilon_\gamma(\rho))$ for every γ. If $x_\gamma \geq y_\gamma > 0$ for all γ, then

$$\Big(\frac{1}{\mathfrak{N}_n} \sum_\gamma x_\gamma^{-1} \Big)^{-1} \geq \Big(\frac{1}{\mathfrak{N}_n} \sum_\gamma y_\gamma^{-1} \Big)^{-1}.$$

Substituting the definition of $\mathcal{H}_q(\rho)$ yields the claimed bound. The zero-violation case follows by continuity. □

The geometric mean enjoys the same monotonicity, so an analogous bound holds for the GTC:

$$\mathcal{T}_q(\rho) \geq \left[\prod_{\gamma \in \Gamma_n} f_{\gamma,q}\big(\epsilon_\gamma(\rho)\big) \right]^{1/\mathfrak{N}_n}.$$

However, the harmonic mean penalizes small $f_{\gamma,q}$ far more severely. This distinction becomes decisive when the witness violations are non-uniform across bipartitions: the HTC bound is dominated by the weakest cut, whereas the GTC bound permits large violations to compensate small ones. Consequently, the HTC-based criterion delivers tighter, more robust characterization of GME for asymmetric mixed states.

We illustrate this contrast for the three-qubit GHZ state mixed with white noise,

$$\rho_{\mathrm{GHZ}}(p) = p\,|\mathrm{GHZ}_3\rangle\langle\mathrm{GHZ}_3| + (1-p)\frac{\mathbb{I}_8}{8}, \qquad p \in [0,1]. \tag{21}$$

All three bipartitions are equivalent, with $\delta_\gamma = 2$ throughout.

HTC bound. A non-decomposable witness constructed via the Choi-Jamiołkowski isomorphism yields the optimal violation $\epsilon(p) = \max\{0, (5p-1)/4\}$ [36, 37]. From this we derive the quadratic bound function

$$f_{\mathrm{HTC}}(p) = \frac{(5p-1)^2}{16\,(2 - 2^{2-q})}.$$

Theorem 3 then gives

$$\mathcal{H}_q\big(\rho_{\mathrm{GHZ}}(p)\big) \geq \mathscr{B}_{\mathrm{HTC}}(p) = \begin{cases} 0, & p \leq \dfrac{1}{5}, \\ \dfrac{(5p-1)^2}{16\,(2-2^{2-q})}, & p > \dfrac{1}{5}. \end{cases} \tag{22}$$

GTC bound. The standard decomposable positive-partial-transpose (PPT) entanglement witness provides the optimal violation $\epsilon(p) = \max\{0, (7p-3)/4\}$ [38,39]. Based on this we compute the linear bound function

$$f_{\mathrm{GTC}}(p) = \frac{2-2^{-(q-2)}}{8}\,(7p-3),$$

leading to

$$\mathcal{T}_q\big(\rho_{\mathrm{GHZ}}(p)\big) \geq \mathscr{B}_{\mathrm{GTC}}(p) = \begin{cases} 0, & p \leq \dfrac{3}{7}, \\ \dfrac{2-2^{-(q-2)}}{8}\,(7p-3), & p > \dfrac{3}{7}. \end{cases} \tag{23}$$

We compare the entanglement detection thresholds, based on SDP entanglement witnesses, of the GTC measure and the proposed HTC measure for the noisy GHZ state, with parameter q ranging from 2 to 16. Figure 1(a) displays the lower bounds $\mathscr{B}_{\mathrm{GTC}}$ and $\mathscr{B}_{\mathrm{HTC}}$ as functions of the mixing parameter p, while Figure 1(b) presents their relative sensitivity $\mathscr{B}_{\mathrm{HTC}}/\mathscr{B}_{\mathrm{GTC}}$ in the two-dimensional contour plot.

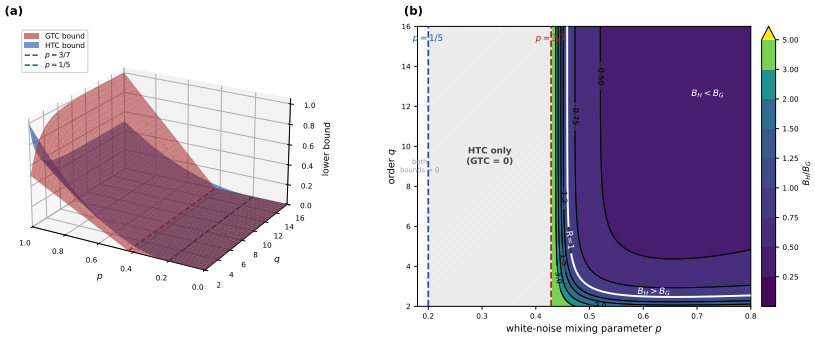


Fig. 1. (a) Lower bounds $\mathscr{B}_{\mathrm{HTC}}$ (blue surface) and $\mathscr{B}_{\mathrm{GTC}}$ (red surface) for $\rho_{\mathrm{GHZ}}(p)$ as functions of p and q. Dashed lines on the p axis mark the detection thresholds $p = 1/5$ (blue) and $p = 3/7$ (red). (b) Contour plot of the relative sensitivity $R = \mathscr{B}_{\mathrm{HTC}}/\mathscr{B}_{\mathrm{GTC}}$ in the (p, q) plane. The hatched gray band $1/5 < p \leq 3/7$ denotes the region where the GTC-type lower bound vanishes while the HTC-type lower bound remains positive. The solid white curve marks $R = 1$, and the labeled black contours give the values of R. Vertical dashed lines indicate $p = 1/5$ and $p = 3/7$.

From Figure 1(a), we observe that the GTC measure built upon a standard decomposable PPT witness detects genuine tripartite entanglement only if $p >$

$3/7 \approx 0.43$, whereas the HTC measure using a non-decomposable witness achieves entanglement identification at the considerably lower threshold $p > 0.2$. The relative sensitivity plot in Figure 1(b) displays $R = \mathscr{B}_{\mathrm{HTC}}/\mathscr{B}_{\mathrm{GTC}}$ in the (p, q) plane. The hatched gray band $1/5 < p \leq 3/7$ marks the region where the GTC-type lower bound vanishes while the HTC-type lower bound remains positive. The solid white curve $R = 1$ and the labeled black contours quantify the enhancement. For $p \in [0.3, 0.6]$ and all displayed values of q, $R > 1$, reaching values between 2 and 5 in the region $p \approx 0.4$, $q \approx 10$. This indicates that the HTC measure is not merely operative over a broader parameter range, but delivers substantially larger lower-bound estimates in the intermediate-noise regime where the GTC bound remains vanishingly small. Therefore, the HTC measure is not only applicable to a wider parameter range but also shows markedly higher sensitivity in the regime where the GTC bound is just emerging from zero, enabling it to detect more entangled states under the same noisy conditions.

To verify that this advantage is not specific to the GHZ state, we apply the same two witness constructions to other paradigmatic multipartite states and to a physically motivated local-noise channel. The resulting detection thresholds are collected in Table 1 and Figure 2.

W state with white noise. Consider

$$\rho_{\mathrm{W}}(p) = p\,|\mathrm{W}_3\rangle\langle\mathrm{W}_3| + (1-p)\frac{\mathbb{I}_8}{8}, \qquad |\mathrm{W}_3\rangle = \frac{1}{\sqrt{3}}(|100\rangle + |010\rangle + |001\rangle). \tag{24}$$

The largest squared overlap of $|\mathrm{W}_3\rangle$ with a biseparable state is $2/3$, so the normalized projector witness is $W_{\mathrm{W}} = \mathbb{I} - \frac{3}{2}|\mathrm{W}_3\rangle\langle\mathrm{W}_3|$. Its expectation is

$$\mathrm{Tr}(W_{\mathrm{W}}\rho_{\mathrm{W}}) = 1 - \frac{3}{2}\frac{1+7p}{8} = \frac{13-21p}{16}, \tag{25}$$

and the GTC-type bound becomes positive only for $p > 13/21 \approx 0.619$. Across each cut, partial transposition produces a block on $\{|000\rangle, |110\rangle, |101\rangle\}$ with diagonal $(1-p)/8$ and two equal off-diagonal entries $p/3$; its smallest eigenvalue is $[3-(3+8\sqrt{2})p]/24$, giving the non-decomposable witness violation $\epsilon(p) = [(3+8\sqrt{2})p-3]/12$ and the HTC-type threshold $p > 3/(3+8\sqrt{2}) \approx 0.210$. Using the same quadratic and linear witness functions as in Eqs. (22)–(23), the two bounds read

$$\begin{aligned}
\mathscr{B}^{\mathrm{W}}_{\mathrm{HTC}}(p) &= \begin{cases} 0, & p \leq \dfrac{3}{3+8\sqrt{2}}, \\ \dfrac{[(3+8\sqrt{2})p-3]^2}{144\,(2-2^{2-q})}, & p > \dfrac{3}{3+8\sqrt{2}}, \end{cases} \\
\mathscr{B}^{\mathrm{W}}_{\mathrm{GTC}}(p) &= \begin{cases} 0, & p \leq 13/21, \\ \dfrac{(2-2^{2-q})(21p-13)}{32}, & p > 13/21. \end{cases}
\end{aligned} \tag{26}$$

At $q = 2$ these are $[(3+8\sqrt{2})p-3]^2/144$ and $(21p-13)/32$, respectively, and are plotted in Figure 2(a): the HTC bound turns on at $p \approx 0.210$ and lies above the

GTC bound throughout most of the region in which the latter is nonzero.

Cluster state with white noise. The four-qubit linear cluster state

$$|\mathrm{Cl}_4\rangle = \frac{1}{2}(|0000\rangle + |0011\rangle + |1100\rangle - |1111\rangle) \tag{27}$$

has inequivalent bipartitions: the four single-particle bipartitions and the bipartition 12|34 have Schmidt rank two, while the bipartitions 13|24 and 14|23 have Schmidt rank four. For the white-noise mixture

$$\rho_{\mathrm{Cl}}(p) = p\,|\mathrm{Cl}_4\rangle\langle\mathrm{Cl}_4| + (1-p)\frac{\mathbb{I}_{16}}{16}, \tag{28}$$

the normalized projector witness is $W_{\mathrm{Cl}} = \mathbb{I} - 2\,|\mathrm{Cl}_4\rangle\langle\mathrm{Cl}_4|$ and

$$\mathrm{Tr}(W_{\mathrm{Cl}}\rho_{\mathrm{Cl}}) = 1 - 2\,\frac{1+15p}{16} = \frac{7-15p}{8}, \tag{29}$$

which detects GME only for $p > 7/15 \approx 0.467$. For the non-decomposable witness, partial transposition on a rank-r bipartition produces a negative eigenvalue of magnitude $p/r - (1-p)/16$, surviving for $p > r/(16+r)$; this gives $p > 1/9$ on rank-two bipartitions and $p > 1/5$ on rank-four bipartitions. Since GME certification requires a positive violation on every bipartition, the two rank-four bipartitions set the HTC threshold at $p > 1/5 = 0.2$. This illustrates the bottleneck principle: bipartitions on which entanglement is detected easily cannot compensate for the hardest bipartitions.

Local depolarizing noise. Imperfect preparation gates act locally. Applying the standard depolarizing channel

$$D_r(\rho) = (1-r)\rho + \frac{r}{2}\,\mathbb{I}_1 \otimes \mathrm{Tr}_1\,\rho \tag{30}$$

to one qubit of $|\mathrm{GHZ}_3\rangle$ produces

$$\rho_r = (1-r)|\mathrm{GHZ}_3\rangle\langle\mathrm{GHZ}_3| + \frac{r}{4}\big(|000\rangle\langle 000| + |011\rangle\langle 011| + |100\rangle\langle 100| + |111\rangle\langle 111|\big), \tag{31}$$

which is normalized for all r. The projector witness expectation is $\mathrm{Tr}(W\rho_r) = (3r-2)/2$, so it certifies GME only for $r < 2/3$. The partial transpose has a block on $\{|100\rangle, |011\rangle\}$ with diagonal $r/4$ and off-diagonal $(1-r)/2$, whose smallest eigenvalue is $(3r-2)/4$; this eigenvalue is negative for $r < 2/3$ and vanishes at $r = 2/3$. The two witnesses therefore cease to detect GME at the same threshold: a local depolarizing channel, unlike global white noise, does not distinguish between the quadratic and linear constructions. At $r = 1$ the state is the separable mixture $\frac{1}{4}(P_{000} + P_{011} + P_{100} + P_{111})$, obtained by fully depolarizing one qubit.

Table 1 and Figure 2(b) show the same pattern for all three states: the HTC-type, non-decomposable witness lowers the detection threshold by a factor between two and three, with the advantage largest for the W state, whose cut distribution is the most non-uniform. For experiments, only a few local measurement settings are

Table 1. GME detection thresholds for three paradigmatic states under white noise, and the maximal local depolarizing strength r tolerated for the GHZ state.

State (noise)	GTC type	HTC type
GHZ_3 + white noise	$3/7 \approx 0.429$	$1/5 = 0.200$
W_3 + white noise	$13/21 \approx 0.619$	$3/(3+8\sqrt{2}) \approx 0.210$
Cl_4 + white noise	$7/15 \approx 0.467$	$1/5 = 0.200$
GHZ_3 + local depolarization (tolerated r)	$2/3 \approx 0.667$	$2/3 \approx 0.667$

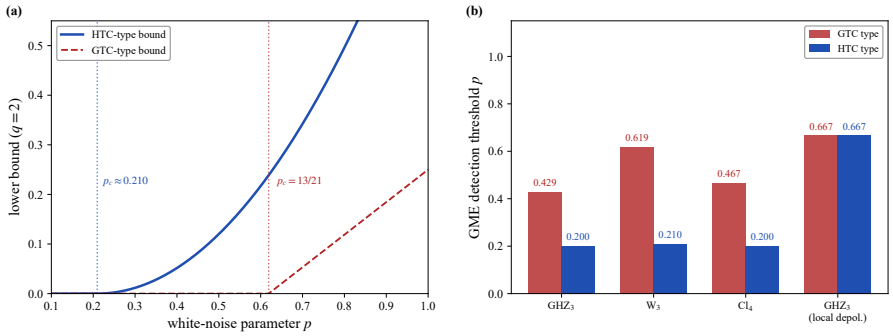


Fig. 2. (a) Witness lower bounds for the white-noise W state at $q = 2$: the HTC-type bound (solid blue) becomes positive at $p \approx 0.210$, the GTC-type bound (dashed red) at $p = 13/21$. (b) GME detection thresholds for white-noise GHZ_3, W_3, Cl_4, and locally depolarized GHZ_3. Red bars: GTC-type witness. Blue bars: HTC-type witness.

needed to evaluate these witness violations, so the thresholds are directly testable on photonic and atomic platforms.

5. Dynamical entanglement generation and degradation

Static noise thresholds do not capture how entanglement evolves in real experiments, where qubits decay during storage and gate operations. We now study three dynamical processes and compare the HTC-type and GTC-type witnesses as functions of time, using the same witness constructions and bound functions as in Sec. 4.

5.1. *Amplitude damping*

Each qubit independently undergoes amplitude damping with rate γ_i. The GHZ coherence $\langle 000|\rho|111\rangle$ decays as $\frac{1}{2}\exp[-\frac{1}{2}(\gamma_1+\gamma_2+\gamma_3)t]$, while the $|111\rangle$ population decays as $\exp[-(\gamma_1+\gamma_2+\gamma_3)t]$ and intermediate excitations are populated at rates determined by the individual γ_i. We compute the exact density matrix using the Kraus representation of the amplitude-damping channel. The GHZ fidelity is

$$F(t) = \frac{1}{4}\Big[1 + \prod_i p_i(t) + \prod_i (1 - p_i(t))\Big] + \frac{1}{2}\prod_i \sqrt{p_i(t)}, \tag{32}$$

where $p_i(t) = e^{-\gamma_i t}$ is the survival probability of the excited state $|1\rangle$ [40]. We verify Eq. (32) against numerical Kraus-map evolution.

Symmetric damping. When $\gamma_1 = \gamma_2 = \gamma_3 = \gamma$, all three cuts remain equivalent at every instant. The GTC-type witness detects GME only while $F(t) > 1/2$, and it ceases to do so at

$$\gamma t_{\mathrm{GTC}}^{\mathrm{death}} = -\ln\left[\left(\frac{\sqrt{10}-1}{3}\right)^2\right] \approx 0.655, \tag{33}$$

obtained by solving $3p + 2\sqrt{p} - 3 = 0$, where $p = e^{-\gamma t}$. The HTC-type bound, by contrast, remains positive for every finite t: for the relevant PPT block, the squared modulus of the off-diagonal element is $c^2 = \frac{1}{4}e^{-3\gamma t}$, while the product of the diagonal entries is $\frac{1}{4}e^{-3\gamma t}(1 - e^{-\gamma t})^3 < c^2$ for all finite t, so its negative eigenvalue never vanishes. Figure 3(a) shows both bounds as functions of γt. At a certification threshold $\mathscr{B}_{\mathrm{th}} = 0.02$, the GTC-type bound falls below threshold at $\gamma t \approx 0.593$ and reaches zero at $\gamma t \approx 0.655$, whereas the HTC-type bound remains above threshold until $\gamma t \approx 0.895$. Thus, under symmetric amplitude damping, the HTC-type witness extends the GME certification range beyond the GTC-type witness, with the practical cutoff set by the chosen certification threshold.

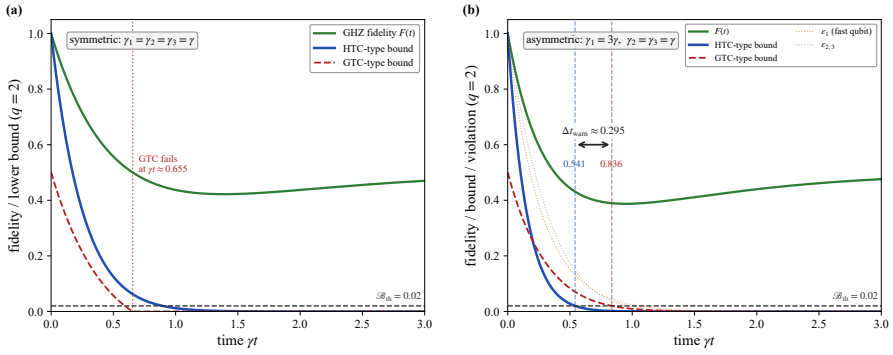


Fig. 3. Amplitude-damping dynamics of GHZ_3 at $q = 2$. (a) Symmetric damping $\gamma_1 = \gamma_2 = \gamma_3 = \gamma$: the green curve is the GHZ fidelity $F(t)$, the solid blue curve is the HTC-type bound, and the dashed red curve is the GTC-type bound. The GTC-type witness fails at $\gamma t \approx 0.655$; the HTC-type witness remains positive for all finite t. The horizontal dashed line marks the certification threshold $\mathscr{B}_{\mathrm{th}} = 0.02$. (b) Asymmetric damping $\gamma_1 = 3\gamma$, $\gamma_2 = \gamma_3 = \gamma$: the HTC-type bound (solid blue, harmonic mean of quadratic per-cut bounds) decays faster than the GTC-type bound (dashed red, geometric mean of linear per-cut bounds). Dotted orange and grey lines show the per-cut PPT violations ϵ_1 (fast qubit) and $\epsilon_{2,3}$. The double-headed arrow marks the early-warning window $\Delta t_{\mathrm{warn}} \approx 0.295$; the horizontal dashed line is the certification threshold $\mathscr{B}_{\mathrm{th}} = 0.02$, and the vertical dashed lines mark the two crossing times $\gamma t = 0.541$ (HTC-type) and $\gamma t = 0.836$ (GTC-type).

Asymmetric damping and the early-warning effect. When one qubit decays faster, the per-cut PPT violations become non-uniform, and the harmonic mean defining the HTC-type bound is dominated by the weakest cut. Figure 3(b) shows

the case $\gamma_1 = 3\gamma$, $\gamma_2 = \gamma_3 = \gamma$. The cut involving the fast qubit decays most rapidly. Both bounds use the same per-cut PPT violations: the HTC-type bound is obtained by taking the harmonic mean of the quadratic witness functions $f_{\mathrm{HTC}}(\epsilon) = \epsilon^2/(2 - 2^{2-q})$, whereas the GTC-type bound is obtained by taking the geometric mean of the linear witness functions $f_{\mathrm{GTC}}(\epsilon) = (2 - 2^{2-q})\epsilon/2$. At $\mathscr{B}_{\mathrm{th}} = 0.02$, the HTC-type bound crosses the threshold at $\gamma t \approx 0.541$, while the GTC-type bound crosses at $\gamma t \approx 0.836$, yielding an early-warning interval

$$\Delta t_{\mathrm{warn}} = t_{\mathrm{GTC}}(\mathscr{B}_{\mathrm{th}}) - t_{\mathrm{HTC}}(\mathscr{B}_{\mathrm{th}}) \approx 0.295, \tag{34}$$

approximately 35% of the GTC-type crossing time. This interval grows with the asymmetry ratio $\gamma_{\max}/\gamma_{\min}$. Thus, under asymmetric damping, the HTC-type witness provides an experimentally useful early-warning signal, with a lead time that increases with the degree of asymmetry and that can be used to halt or refresh the state before the GTC-type bound falls below threshold.

5.2. *Pure dephasing*

Under independent pure dephasing with rates χ_i, the diagonal populations are preserved while the coherences decay as $\langle 000|\rho(t)|111\rangle = \frac{1}{2}\exp[-(\chi_1 + \chi_2 + \chi_3)t]$ [41]. The fidelity is

$$F(t) = \frac{1}{2}\big[1 + e^{-(\chi_1+\chi_2+\chi_3)t}\big]. \tag{35}$$

For symmetric dephasing $\chi_i = \chi$, $F(t) = \frac{1}{2}(1 + e^{-3\chi t})$. The PPT and projector-witness violations coincide, $\epsilon(t) = e^{-3\chi t}$, but the resulting bounds differ because the witness functions are different: $\mathscr{B}_{\mathrm{HTC}} = \epsilon^2 = e^{-6\chi t}$ (quadratic) and $\mathscr{B}_{\mathrm{GTC}} = \epsilon/2 = \frac{1}{2}e^{-3\chi t}$ (linear), so that $\mathscr{B}_{\mathrm{HTC}}/\mathscr{B}_{\mathrm{GTC}} = 2\epsilon = 2e^{-3\chi t}$. Both bounds remain strictly positive for all finite t, but they decay at different rates, as shown in Figure 4(a). Thus, under pure dephasing, the HTC-type bound is the more stringent bottleneck-sensitive witness, decaying twice as fast as the GTC-type bound, although neither vanishes at finite time. Under asymmetric dephasing the same bottleneck effect appears: the cut across which phase coherence decays fastest determines the HTC-type bound.

5.3. *Finite-duration gate generation*

We now turn to entanglement generation itself, which is more demanding. We prepare GHZ_3 from $|000\rangle$ using the circuit

$$\mathrm{Had}(q_0) \to \mathrm{CNOT}(q_0 \to q_1) \to \mathrm{CNOT}(q_0 \to q_2),$$

where q_0, q_1, q_2 label the three qubits. Each ideal gate U_j has duration t_{gate}. Independent amplitude damping acts on qubit i with rate γ_i, described by the lowering operator $\sigma_-^{(i)} = |0\rangle_i\langle 1|$. The evolution is governed by

$$\frac{d\rho}{dt} = -i[H(t), \rho] + \sum_{i=1}^{3} \gamma_i \, \mathcal{D}[\sigma_-^{(i)}]\rho, \qquad \mathcal{D}[L]\rho = L\rho L^\dagger - \frac{1}{2}\{L^\dagger L, \rho\}, \tag{36}$$

where $H(t)$ is the piecewise-constant Hamiltonian that implements the gate sequence [42]. For each gate interval, the ideal gate U_j is realized by $H_j = (i/t_{\text{gate}}) \log U_j$, with the matrix logarithm chosen so that H_j is Hermitian, and hence $\exp(-iH_j t_{\text{gate}}) = U_j$. We solve the master equation exactly for piecewise-constant $H(t)$ by vectorizing ρ and exponentiating the Liouvillian superoperator on each gate interval, ensuring continuity of the density matrix at the gate boundaries.

Let $F(t) = \langle \text{GHZ}_3 | \rho(t) | \text{GHZ}_3 \rangle$ be the GHZ fidelity, and let $\mathscr{B}_{\text{HTC}}$ and $\mathscr{B}_{\text{GTC}}$ denote the SDP-witness lower bounds of Sec. 4. Figure 4(b) shows the dynamics for symmetric damping $\gamma_i = \gamma$ with $\gamma t_{\text{gate}} = 0.15$, i.e. $T_1 = 1/\gamma \approx 6.7\, t_{\text{gate}}$. At the end of the sequence, $F \approx 0.783$, $\mathscr{B}_{\text{HTC}} \approx 0.444$, and $\mathscr{B}_{\text{GTC}} \approx 0.283$. The fidelity starts at $1/2$ (the overlap of $|000\rangle$ with $|\text{GHZ}_3\rangle$), dips during the Hadamard and first CNOT, and recovers as the second CNOT completes the GHZ state. Both lower bounds remain near zero until the final gate and then rise together. For $\gamma t_{\text{gate}} \in [0, 0.5]$, both bounds stay positive; at $\gamma t_{\text{gate}} = 0.5$, $F = 0.577$, $\mathscr{B}_{\text{HTC}} = 0.073$, and $\mathscr{B}_{\text{GTC}} = 0.077$. Thus the practical limit is determined by the desired certification threshold rather than by a hard cutoff. Because the HTC-type bound emphasizes the weakest cut, under asymmetric damping (e.g., when one qubit has a shorter T_1) it can signal the optimal certification time slightly before the nominal circuit end. Overall, the HTC-type bound provides a practical, experimentally accessible early certification signal for finite-duration GME generation.

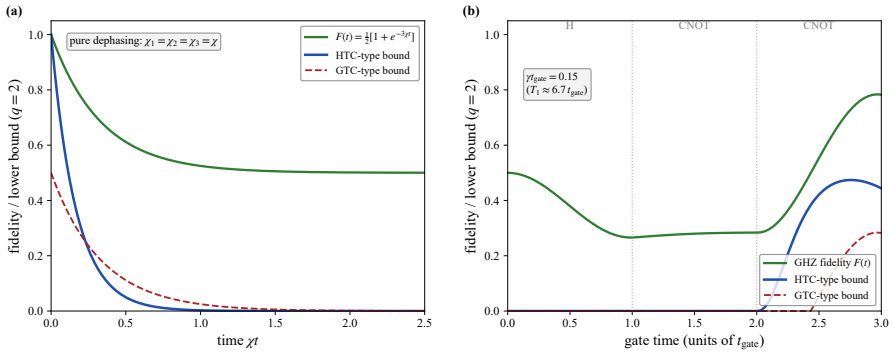


Fig. 4. (a) Pure dephasing of GHZ_3 at $q = 2$ with $\chi_1 = \chi_2 = \chi_3 = \chi$. The green curve is $F(t) = \frac{1}{2}(1 + e^{-3\chi t})$; the blue solid curve is the HTC-type bound $\mathscr{B}_{\text{HTC}} = e^{-6\chi t}$, and the red dashed curve is the GTC-type bound $\mathscr{B}_{\text{GTC}} = \frac{1}{2} e^{-3\chi t}$. Both remain positive for all finite t. (b) GHZ_3 generation via Had $\to$ CNOT $\to$ CNOT with amplitude damping $\gamma t_{\text{gate}} = 0.15$. The green curve is the GHZ fidelity; the blue and red curves are the HTC-type and GTC-type bounds. Vertical dotted lines mark gate boundaries. Both bounds turn on only during the final CNOT, when genuine tripartite entanglement is established.

6. Entanglement ordering with HTC

Distinct GME measures generally induce different orderings on the set of states, even within the same Stochastic Local Operations and Classical Communication (S-LOCC) equivalence class [43–47]. Since the HTC $\mathcal{H}_q$ computes the harmonic mean of the entanglement distribution $\{\mathfrak{T}_q^{(\gamma)}\}_{\gamma\in\Gamma_n}$, it is far more sensitive to distributional non-uniformity than measures constructed from the geometric mean or the minimum value. In this section, we prove this ordering inequivalence analytically and introduce a dimensionless parameter that captures the non-uniformity of the entanglement distribution independently of the overall entanglement strength.

6.1. *Inequivalence with geometric and minimum-based measures*

We consider the bipartite q-concurrence $\mathfrak{T}_q^{(\gamma)}$ for each cut γ. For a single-qubit reduced density matrix with eigenvalues $\{\lambda, 1-\lambda\}$, this measure is a strictly increasing function of $\lambda(1-\lambda)$ and vanishes if and only if the reduced state is pure. Since subsequent ordering comparisons depend only on the relative magnitudes of bipartite entanglements, we only need to demonstrate this inequivalence for the standard concurrence ($q=2$), for which $\mathfrak{T}_2^{(\gamma)} = 2(1-\operatorname{Tr}\rho^2) = 4\lambda(1-\lambda)$; identical conclusions then carry over to any $q>0$ via monotonicity.

Consider the following two families of three-qubit pure states:

$$|\Psi(\theta,\phi)\rangle = \cos\theta\,|000\rangle + \sin\theta\cos\phi\,|011\rangle + \sin\theta\sin\phi\,|101\rangle, \tag{37}$$

$$|\Phi(\theta)\rangle = \cos\theta\,|000\rangle + \sin\theta\,|111\rangle. \tag{38}$$

For $|\Phi(\theta)\rangle$ every single-qubit reduction has eigenvalues $\{\cos^2\theta, \sin^2\theta\}$, so the three bipartite concurrences are identical:

$$C_\Phi(\theta) = 2|\cos\theta\sin\theta|. \tag{39}$$

For $|\Psi(\theta,\phi)\rangle$ the marginal eigenvalues are $\{\sin^2\theta\sin^2\phi,\ 1-\sin^2\theta\sin^2\phi\}$ (first qubit), $\{\sin^2\theta\cos^2\phi,\ 1-\sin^2\theta\cos^2\phi\}$ (second qubit), and $\{\sin^2\theta, \cos^2\theta\}$ (third qubit). The corresponding concurrences are denoted $C_1(\theta,\phi)$, $C_2(\theta,\phi)$ and $C_3(\theta)$; note that $C_3(\theta) = C_\Phi(\theta)$ and $C_2(\theta,\phi) = C_1(\theta, \frac{\pi}{2}-\phi)$.

Inequivalence between HTC and GTC. We construct a pair of states for which the GTC $\mathcal{T}$ and the HTC $\mathcal{H}$ yield opposite orderings. Choose $\theta = \pi/3$ and ϕ^* satisfying $\sin^2\phi^* = 2/3$ (i.e. $\phi^* \approx 0.955\,\text{rad}$). Then

$$C_1(\pi/3,\phi^*) = \sqrt{3}\sin\phi^*\sqrt{1-\tfrac{3}{4}\sin^2\phi^*} = 1, \tag{40}$$

$$C_2(\pi/3,\phi^*) = \sqrt{3}\cos\phi^*\sqrt{1-\tfrac{3}{4}\cos^2\phi^*} = \frac{\sqrt{3}}{2} \approx 0.866, \tag{41}$$

$$C_3(\pi/3) = \frac{\sqrt{3}}{2} \approx 0.866. \tag{42}$$

Therefore, we obtain the geometric and harmonic means for $|\Psi(\pi/3, \phi^*)\rangle$ as

$$\mathcal{T}(|\Psi\rangle) = \big(C_1 C_2 C_3\big)^{1/3} \approx 0.9086, \qquad \mathcal{H}(|\Psi\rangle) = \frac{3}{C_1^{-1} + C_2^{-1} + C_3^{-1}} \approx 0.9065. \tag{43}$$

Now take $|\Phi(\theta')\rangle$ with $\theta' = \frac{1}{2}\arcsin(0.9075)$, so that $C_\Phi(\theta') = 0.9075$. This state is completely uniform, hence

$$\mathcal{T}(|\Phi\rangle) = \mathcal{H}(|\Phi\rangle) = 0.9075. \tag{44}$$

Comparing the two measures we obtain

$$\mathcal{T}(|\Psi\rangle) \approx 0.9086 \ > \ 0.9075 = \mathcal{T}(|\Phi\rangle), \qquad \mathcal{H}(|\Psi\rangle) \approx 0.9065 \ < \ 0.9075 = \mathcal{H}(|\Phi\rangle). \tag{45}$$

Thus GTC ranks $|\Psi\rangle$ as more entangled whereas HTC ranks $|\Phi\rangle$ as more entangled, proving the two measures are inequivalent.

Inequivalence between HTC and GMC. The GMC is $C_{\mathrm{GME}} = \min_\gamma \mathfrak{T}_q^{(\gamma)}$ [18]. Choose $\theta = \pi/3$ and $\phi = \pi/4$. Then

$$C_\Phi(\pi/3) = \frac{\sqrt{3}}{2} \approx 0.866. \tag{46}$$

For $|\Psi(\pi/3, \pi/4)\rangle$ we have the concurrences are

$$C_3 = \frac{\sqrt{3}}{2} \approx 0.866, \qquad C_1 = C_2 = \frac{\sqrt{15}}{4} \approx 0.968. \tag{47}$$

Hence $C_{\mathrm{GME}}(|\Psi\rangle) = C_{\mathrm{GME}}(|\Phi\rangle) = \sqrt{3}/2$. The harmonic mean of $|\Psi\rangle$ satisfies

$$\mathcal{H}(|\Psi\rangle) = \frac{3}{\frac{2}{C_1} + \frac{1}{C_3}} > \frac{3}{\frac{3}{C_3}} = C_3 = \frac{\sqrt{3}}{2} = \mathcal{H}(|\Phi\rangle). \tag{48}$$

Consequently, the GMC cannot distinguish the two states, whereas the HTC can.

6.2. *Entanglement non-uniformity parameter*

The discrepancies shown above arise because $\mathcal{H}_q$ and $\mathcal{T}_q$ respond with different sensitivities to heterogeneity in the bipartite entanglement distribution $\{\mathfrak{T}_q^{(\gamma)}\}_{\gamma\in\Gamma_n}$.

To quantify the heterogeneity of the entanglement distribution irrespective of the overall entanglement scale, we define the entanglement non-uniformity parameter

$$\eta_q(|\psi\rangle) \equiv \frac{\mathcal{T}_q(|\psi\rangle)}{\mathcal{H}_q(|\psi\rangle)} \geq 1, \tag{49}$$

where the inequality follows from the geometric-harmonic mean inequality. Equality $\eta_q(|\psi\rangle) = 1$ is attained if and only if all bipartite q-concurrences $\mathfrak{T}_q^{(\gamma)}$ are equal, which corresponds to a perfectly uniform distribution of entanglement across all cuts. For a biseparable state one cut has $\mathcal{H}_q = 0$, and we adopt $\eta_q = +\infty$.

The extremal cases admit a transparent physical interpretation.

- $\eta_q = 1$ occurs when all bipartite reductions produce the same entanglement. For instance, the n-qubit $|\mathrm{GHZ}_n\rangle$ state: every nontrivial bipartition yields a rank-2 reduced state with eigenvalues $\{1/2, 1/2\}$, so the entanglement distribution is perfectly uniform. The four-qubit cluster state also has $\eta_q = 1$ because every cut is maximally entangled within its Schmidt rank.
- $\eta_q \gg 1$ signals a severe bottleneck. For the W state, a cut separating k qubits gives $\mathfrak{T}_2^{(k)} = 4k(n-k)/n^2$, which depends on k, so $\eta_2(|\mathrm{W}_n\rangle)$ grows with n (Fig. 5), reflecting the fragility of W-type entanglement under subsystem loss.

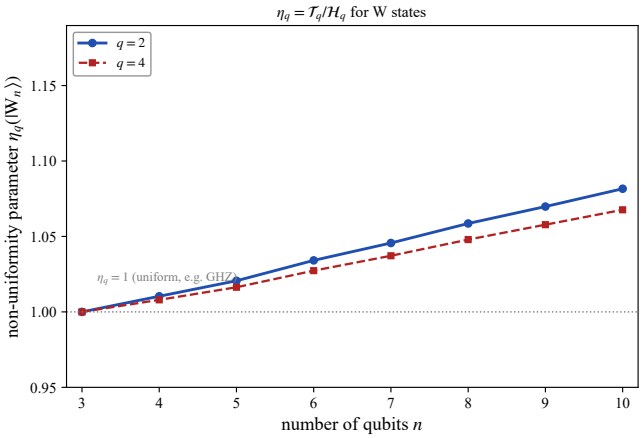


Fig. 5. Non-uniformity parameter $\eta_q = \mathcal{T}_q/\mathcal{H}_q$ for n-qubit W states at $q = 2$ (blue circles) and $q = 4$ (red squares). The dotted grey line at $\eta_q = 1$ corresponds to perfectly uniform states such as GHZ. The growth with n quantifies the increasing bottleneck severity of W-type entanglement.

Theorem 4. *Let $|\psi\rangle$ be a genuinely multipartite entangled pure state, and let $\{x_\gamma\}_{\gamma\in\Gamma_n}$ denote its entanglement distribution. Define $\bar{x} = \mathcal{A}(|\psi\rangle)$ as the arithmetic mean, and set the relative deviations $\varepsilon_\gamma = \frac{x_\gamma}{\bar{x}} - 1$. If these deviations are small, then*

$$\eta_q(|\psi\rangle) = 1 + \frac{1}{2\mathfrak{N}_n} \sum_{\gamma\in\Gamma_n} \varepsilon_\gamma^2 + O(\delta^3), \tag{50}$$

where $\delta = \max_{\gamma\in\Gamma_n} |\varepsilon_\gamma|$.

Proof. Write $x_\gamma = \bar{x}(1+\varepsilon_\gamma)$ with $\sum_\gamma \varepsilon_\gamma = 0$ and $|\varepsilon_\gamma| \le \delta$. Expanding the geometric and harmonic means gives

$$\mathcal{T}_q = \bar{x} \prod_\gamma (1+\varepsilon_\gamma)^{1/\mathfrak{N}_n} = \bar{x}\Big[1 - \frac{1}{2\mathfrak{N}_n} \sum_\gamma \varepsilon_\gamma^2 + O(\delta^3)\Big], \tag{51}$$

$$\mathcal{H}_q = \bar{x}\Big[\frac{1}{\mathfrak{N}_n}\sum_{\gamma}(1+\varepsilon_\gamma)^{-1}\Big]^{-1} = \bar{x}\Big[1-\frac{1}{\mathfrak{N}_n}\sum_{\gamma}\varepsilon_\gamma^2+O(\delta^3)\Big]. \tag{52}$$

Taking the ratio yields the claimed expression. □

The theorem above demonstrates that, in the small-deviation limit, $\eta_q - 1$ is proportional to the variance of the relative deviations. A value close to unity reflects a nearly uniform entanglement distribution. In this case, all bipartitions yield comparable entanglement values, and no single bipartition constitutes a bottleneck. However, the unique strength of the HTC manifests for strongly inhomogeneous entanglement distributions, especially when several x_γ lie well below the mean. In such cases, the higher-order terms in the expansion cannot be neglected. The harmonic mean responds strongly to the smallest entries and falls rapidly, which increases η_q. Thus, large η_q signals weak bipartitions that may act as bottlenecks in quantum networks. This nonlinear sensitivity makes the HTC preferable to measures based on the arithmetic mean and the geometric mean for detecting weak bipartitions.

7. Conclusion

In this paper, we have introduced the HTC, a GME measure constructed as the harmonic mean of the total concurrence over all nontrivial bipartitions. This measure vanishes whenever any single bipartition becomes separable, satisfies all standard axioms for GME, and yields strictly larger values for GHZ states than for W states. The HTC is not an isolated construction but the bottleneck-sensitive member of a full one-parameter family of power-mean total concurrences. We have shown that all members of this family with nonpositive power parameters are valid genuine multipartite entanglement measures, while members with positive power parameters fail to correctly identify biseparable states.

For mixed states, we derive computable lower bounds from SDP-based entanglement witnesses. For white-noise mixtures of canonical multipartite states, the HTC-based witness certifies GME at lower state purity than the witness corresponding to the GTC. A local depolarizing channel acting on a single qubit renders both types of witnesses ineffective at the same noise strength. We have analyzed the performance of these witnesses under three typical dynamical processes. The HTC-type witness certifies entanglement over a markedly longer time interval than the GTC-type witness. Under asymmetric dissipation, the bottleneck sensitivity of HTC provides early warning of impending entanglement loss. For finite-duration entanglement generation with dissipation, the practical detection limit is determined by the chosen certification threshold, and HTC naturally identifies the optimal time for entanglement verification. The entanglement ordering induced by the HTC is inequivalent to those from both the GTC and the GMC. This distinction originates from the strong response of the harmonic mean to inhomogeneity in the entanglement distribution across bipartitions. We also introduce a dimensionless

non-uniformity parameter to quantify such unevenness of the entanglement distribution.

The witness-based detection scheme requires only a small set of local measurement settings, which makes the measure experimentally viable on photonic, atomic, and optomechanical platforms. Extensions of this framework to continuous-variable systems and more general dynamical entanglement generation scenarios represent promising directions for future work.

Author contributions

In this paper, Q.H. is responsible for content and structure, X.H. is responsible for text inputting, J.L. and X.W. are responsible for references searching.

Conflict of Interests

There is no conflict of interest, financial or non-financial, between the authors.

Acknowledgements

This research is supported by National Natural Science Foundation of China (grant numbers 62261049;12261080), Funds for Innovative Fundamental Research Group Project of Gansu Province (grant number 25JRRA002) and Gansu Provincial "Innovation Star" Project Fund for University Graduate Students (grant number pending).

Data Availability

Data sharing is not applicable to this paper as no data sets were generated or analyzed during the current study.

References

1. Ekert A K 1991 *Phys. Rev. Lett.* **67** 661
2. Bennett C H, Brassard G and Mermin N D 1992 *Phys. Rev. Lett.* **68** 557
3. Bennett C H, Brassard G, Crépeau C, Jozsa R, Peres A and Wootters W K 1993 *Phys. Rev. Lett.* **70** 1895
4. Liu B, Zhang J, Qiu S and Zhang M 2025 *Chin. Phys. B* **34** 030304
5. Raussendorf R and Briegel H J 2001 *Phys. Rev. Lett.* **86** 5188
6. Briegel H J, Browne D E, Dür W, Raussendorf R and den Nest M V 2009 *Nature Physics* **5** 19
7. Amico L, Fazio R, Osterloh A and Vedral V 2008 *Rev. Mod. Phys.* **80** 517
8. Vedral V, Plenio M B, Rippin M A and Knight P L 1997 *Phys. Rev. Lett.* **78** 2275
9. Horodecki R, Horodecki P, Horodecki M and Horodecki K 2009 *Rev. Mod. Phys.* **81** 865
10. Hill S A and Wootters W K 1997 *Phys. Rev. Lett.* **78** 5022
11. Wootters W K 1998 *Phys. Rev. Lett.* **80** 2245
12. Vidal G and Werner R F 2002 *Phys. Rev. A* **65** 032314

13. Chen K, Albeverio S and Fei S M 2005 *Phys. Rev. Lett.* **95** 040504
14. Yang X, Luo M X, Yang Y H and Fei S M 2021 *Phys. Rev. A* **103** 052423
15. Wei Z W and Fei S M 2022 *J. Phys. A: Math. Theor.* **55** 275303
16. Wei T C and Goldbart P M 2003 *Phys. Rev. A* **68** 042307
17. Sen(De) A and Sen U 2010 *Phys. Rev. A* **81** 012308
18. Ma Z H, Chen Z H, Chen J L, Spengler C, Gabriel A and Huber M 2011 *Phys. Rev. A* **83** 062325
19. Li Y F and Shang J W 2022 *Phys. Rev. Research* **4** 023059
20. Shi X and Chen L 2023 *Ann. Phys. (Berlin)* **535** 2300305
21. Xie S and Eberly J H 2021 *Phys. Rev. Lett.* **127** 040403
22. Jin Z X, Li-Jost X Q, Fei S M and Qiao C F 2023 *Phys. Rev. A* **107** 012409
23. Li H, Gao T and Yan F L 2024 *Phys. Rev. A* **109** 012213
24. Wang K K, Wei Z W and Fei S M 2025 *Eur. Phys. J. Plus* **140** 374
25. Xuan D P, Shen Z X, Zhou W, Wang Z X and Fei S M 2025 *Adv. Quantum Technol.* **8** 2500149
26. Liang R Z, Liu X and Jin Z X 2026 *Annalen der Physik* **538** e00554
27. de Andrade M G, Milligen E A V, Bacciottini L, Chandra A, Pouryousef S, Panigrahy N K, Vardoyan G and Towsley D 2024 arXiv:2405.18252 [quant-ph]
28. Gühne O and Tóth G 2009 *Phys. Rep.* **474** 1
29. Cai Q Z, Fan B Y, Fan Y R, Deng G W, Wang Y, Song H Z, Guo G C and Zhou Q 2024 *Chin. Phys. Lett.* **41** 114201
30. Lahlou Y, Maroufi B and Daoud M 2024 *Chin. Phys. B* **33** 050303
31. Doherty A C, Parrilo P A and Spedalieri F M 2004 *Phys. Rev. A* **69** 022308
32. Doherty A C, Parrilo P A and Spedalieri F M 2005 *Phys. Rev. A* **71** 032333
33. Mintert F 2007 *Phys. Rev. A* **75** 052302
34. Gühne O, Reimpell M and Werner R F 2008 *Phys. Rev. A* **77** 052317
35. Shi X 2024 arXiv:2312.17620 [quant-ph]
36. Choi M D 1975 *Linear Algebra Appl.* **10** 285
37. Jamiołkowski A 1972 *Rep. Math. Phys.* **3** 275
38. Peres A 1996 *Phys. Rev. Lett.* **77** 1413
39. Horodecki M, Horodecki P and Horodecki R 1996 *Phys. Lett. A* **223** 1
40. Batin A Q, Chand S, Sk R and Panigrahi P K 2026 arXiv:2609.07084 [quant-ph]
41. Nielsen M A and Chuang I L 2001 *Quantum Computation and Quantum Information* (Cambridge: Cambridge University Press)
42. Lindblad G 1976 *Commun. Math. Phys.* **48** 119
43. Dür W, Vidal G and Cirac J I 2000 *Phys. Rev. A* **62** 062314
44. Verstraete F, Dehaene J, Moor B D and Verschelde H 2002 *Phys. Rev. A* **65** 052112
45. Nielsen M A 1999 *Phys. Rev. Lett.* **83** 436
46. Życzkowski K and Bengtsson I 2002 *Ann. Phys. (N.Y.)* **295** 115
47. Plenio M B and Virmani S 2007 *Quantum Inf. Comput.* **7** 1